Brownian fluctuations of an optically rotated nanorod

(article starts on next page)

optica

Brownian fluctuations of an optically rotated nanorod

Faegheh Hajizadeh,[1,2,†] Lei Shao,[1,†,*] Daniel Andrén,[1] Peter Johansson,[1,3] Halina Rubinsztein-Dunlop,[1,4] and Mikael Käll[1]

[1]Department of Physics, Chalmers University of Technology, 412 96 Göteborg, Sweden
[2]Department of Physics, Institute for Advanced Studies in Basic Sciences, Zanjan 45195-1159, Iran
[3]School of Science and Technology, Örebro University, 701 82 Örebro, Sweden
[4]Quantum Science Laboratory, School of Mathematics and Physics, The University of Queensland, Brisbane, QLD 4072, Australia
*Corresponding author: lei.shao@chalmers.se

Gold nanorods can be optically trapped in aqueous solution and forced to rotate at kilohertz rates by circularly polarized laser light. This enables detailed investigations of local environmental parameters and processes, such as medium viscosity and nanoparticle–molecule reactions. Future applications may include nanoactuation and single-cell analysis. However, the influence of photothermal heating on the nanoparticle dynamics needs to be better understood in order to realize widespread and quantitative use. Here we analyze the hot Brownian motion of a rotating gold nanorod trapped in two dimensions by an optical tweezers using experiments and stochastic simulations. We show that, for typical settings, the effective rotational and translational Brownian temperatures are drastically different, being closer to the nanorod surface temperature and ambient temperature, respectively. Further, we show that translational dynamics can have a non-negligible influence on the rotational fluctuations due to the small size of a nanorod in comparison to the focal spot. These results are crucial for the development of gold nanorods into generic and quantitative optomechanical sensor and actuator elements.   © 2017 Optical Society of America

OCIS codes: (350.4855) Optical tweezers or optical manipulation; (240.6680) Surface plasmons; (160.4236) Nanomaterials; (280.6780) Temperature.

https://doi.org/10.1364/OPTICA.4.000746

1. INTRODUCTION

The motion of a Brownian particle in solution is strongly affected by thermal agitation from collisions with the surrounding fluid molecules, resulting in well-defined random dynamics dependent on fluid temperature and viscosity. Optical tweezers offer an ideal platform to study Brownian dynamics because the focused laser field introduces deterministic optical forces and torques [1–5]. By recording the movement of a trapped Brownian particle, it is possible to probe local environmental properties such as viscosity [6] and temperature [7]. A trapped particle can further work as a handle to analyze and control biomolecules, enabling detailed biophysical measurements [8–10].

Gold nanocrystals are highly interesting from the point of view of optical manipulation and studies of Brownian dynamics because they are biocompatible and support very strong light–matter interactions due to the well-known surface plasmon resonance phenomenon. Consequently, a number of studies on optically trapped colloidal Au nanocrystals have been reported in the literature [11–17]. The large electric dipole polarizability associated with plasmon excitation in fact results in optical forces and torques that are enhanced to such an extent that Au particles as small as ~10 nm can be trapped [18] and gold nanorods can be

propelled to spin at rotation frequencies up to more than 40 kHz by angular momentum transfer from circular polarized light [19]. Together with their superior refractometric sensing and local field-enhancement properties, these features make Au nanocrystals potential generic optomechanical sensor and actuator elements. However, plasmon excitation also leads to strongly enhanced electromagnetic fields within the metal nanoparticle, and this in turn leads to photothermal heating effects that can be orders of magnitude stronger than for dielectric particles of similar size [20]. Plasmonic heating can be an advantage or a detriment, depending on the specific application. It is usually a problem in studies of biological cells and tissues, where a small change in temperature can strongly affect intracellular processes [21], biomolecular transitions [22], and local force measurements [9], but it can be very useful in applications like drug release [23], gene regulation [21], photothermal therapy [24,25], and thermophoretic trapping [26]. Naturally, photothermal effects are of particular concern in applications based on optical manipulation since the light intensities involved are then typically very high. Though challenging, measurements of the medium temperature around optically trapped gold nanocrystals are therefore of both

fundamental interest and great importance for the development of various applications.

In this work, we elucidate the Brownian dynamics of gold nanorods that are trapped and rotated at high frequency in a 2D optical trap formed by a circular polarized focused laser beam with a wavelength close to the main plasmon resonance wavelength of the particles. Due to photothermal heating, the trapped nanoparticle has a much higher surface temperature than the average temperature of the surrounding water solution. The resulting temperature gradient then leads to so-called hot Brownian motion [27–29]. By simultaneously studying the translations and rotation of a particle, while taking into account the spatially heterogeneous temperature-dependent solvent viscosity [30] and actual particle position within the laser focus, we show that the effective Brownian temperatures, T_r and T_t, characterizing rotational and translational degrees of freedom, respectively, are drastically different. The analysis we present is applicable to various other types of light-absorbing particles and therefore relevant to a wide range of applications based on optical manipulation.

2. EXPERIMENTS

The experimental setup [Fig. 1(a)] used here is similar to that described in Ref. [19], but with the additional feature of being able to probe real-time nanoparticle lateral displacement (x, y) in the optical trap using a quadrant photodiode (QPD). We prepared gold nanorods with an average size of (84 ± 5) nm × (164 ± 10) nm in aqueous solution according to Ref. [19] [Fig. 1(a) inset]. The gold nanorod sample has a plasmon resonance centered at 760 nm in solution and the trapping laser wavelength is 830 nm. A combination of a half-wave and quarter-wave plate was employed to create an almost perfect circular polarization in the laser trap [31]. The comparatively large scattering cross-section of the gold nanorods boosts transfer of both angular and linear momentum. The latter results in strong radiation

Fig. 1. Measurement of the rotation dynamics of a 2D trapped gold nanorod. (a) Schematic of the optical tweezers setup. (Inset) Scanning electron microscopy image of the used gold nanorods. (b) Measured QPD voltage dependence on immobilized nanorod displacement from the laser focus at different laser powers. The dashed line shows a fit to the central linear range of the data measured at 11.7 mW. (c) and (d) QPD-measured trajectory of a rotating nanorod in the optical trap (c) and distribution of the rod position (d). The laser power was set at 6.4 mW. (e) PSD of the measured nanorod x displacement. The red smooth curve is the fitting at $f \ll f_{avg}$ to obtain the corner frequency.

pressure, which makes it challenging to achieve stable optical trapping in 3D. As a result, the gold nanorods are trapped in 2D against a glass slide and rotated about their short axis in a plane normal to the optical axis [19]. The back-scattered laser light from the trapped particle is split into two beams. One of the beams is recorded by the QPD (First Sensor), located at the objective back focal plane [32,33], and the other beam is passed through a linear polarizer and collected by a fiber-coupled avalanche photodiode (APD) connected to a hardware autocorrelator (ALV-5000). This setup can be used to measure both translational and rotational Brownian motion dynamics of a trapped nanoparticle with high temporal and spatial resolution [32,34].

The QPD gives three output voltage signals, V_{total}, V_x, and V_y, indicating both total back-scattered laser intensity reaching the detector (V_{total}) and the displacement of a nanoparticle in the optical trap with respect to the laser focus (V_x, V_y) [18]. V_x and V_y can be converted to particle position in order to track translational Brownian motion [18]. The conversion was based on calibration measurements using individual immobilized nanorods (Section 1 of Supplement 1) [32,33] that were scanned through the laser focus using an XY piezoelectric scanning stage [Fig. 1(b)]. V_x, and V_y are linearly proportional to the particle displacements, $V_x = bx$, $V_y = by$, when the nanorod is within ~250 nm from the laser focus and varies with laser power. Unfortunately, for a fixed laser power, b also varies between different nanorods because of their varying resonant scattering properties, which are highly sensitive to the absolute size and shape. We found that the measured b for different nanorods displayed a variance less than 15% for fixed laser power. Figures 1(c) and 1(d) show the trajectory and corresponding displacement distribution, respectively, of a rotating gold nanorod obtained using the average b value from measurements on several immobilized nanorods. The particle displacement follows a Gaussian distribution centered at the laser focus, as expected. According to an harmonic approximation of the optical trapping potential, the standard deviation of the particle lateral displacement σ is expected to follow $\sigma = (k_B T_t / k)^{1/2}$, where k is the trap stiffness (force constant). We also calculated the power spectral density (PSD) of the measured nanorod displacement [Fig. 1(e)]. The PSD can be used to obtain the corner frequency f_c, which is determined by the trap stiffness k and the nanorod translational friction coefficient $\gamma_t(T_t)$ through $f_c = k/(2\pi\gamma_t)$, via a fit to PSD$(f) = C/(f^2 + f_c^2)$ [35]. Since the conversion factor b is now included in the fitting parameter C, we can estimate f_c directly from the PSD of V_x or V_y without converting to absolute displacement. The intensity profile in the laser focus can also be obtained from the calibration experiment via a fit of the measured $V_{total}(x, y)$ to a Gaussian function. This measurement is quite robust since it is independent of the absolute laser power and properties of the immobilized nanoparticle. We obtained a laser beam waist size $w_0 \approx 541$ nm for the present experiment. The beam waist and corner frequency are the main experimental parameters used for estimating the translational Brownian temperature, as discussed further below.

Since the dichroic mirror in the setup has different reflectivity to s- and p-polarized light, the PSD data also reveals the rotational motion of a trapped anisotropic particle. For an object with two-fold symmetry, like a nanorod, the PSD will exhibit a peak centered at $f_{QPD} = 2f_{avg}$, where f_{avg} is the average rotation frequency in the trap. Although the rotation peak is clearly visible in the trace displayed in Fig. 1(e), it is much more obvious in the
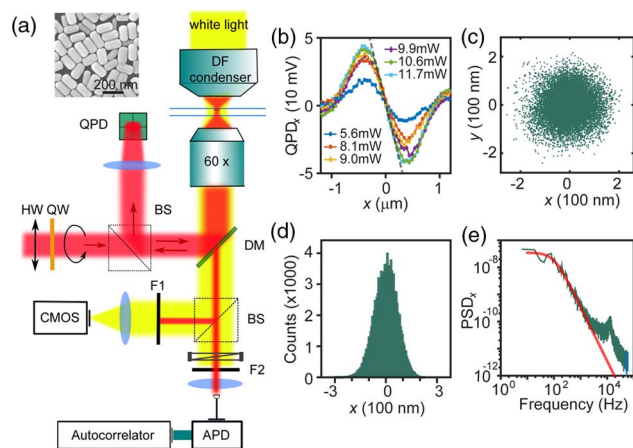
PSD of V_{total}, shown in Fig. 2(a). A peak fit to a Lorentzian function can be used to determine the peak width Γ, which describes the fluctuation in rotation frequency. Note that the appearance of a rotational peak in the PSD of V_x or V_y implies that the fit to obtain the corner frequency has to be performed for $f \ll f_{QPD}$.

The rotational motion of the nanorod can also be independently analyzed through the APD/autocorrelator setup. The intensity of the total back-scattered light emanating from the nanorod, after passing through a linear polarizer, is $I_{sca}^P = \sigma_{sca,CP} I(x, y) \cos^2 \varphi$. Here, $\sigma_{sca,CP}$ is the nanorod scattering cross-section for circular polarization at the laser wavelength, $I(x, y)$ is the laser intensity at the particle position, and φ is the rotation angle of the nanorod relative to the polarizer [19,36]. The autocorrelation function (ACF) of I_{sca}^P, which is directly obtained from the hardware autocorrelator [Fig. 2(b)], can be fitted

Fig. 2. Experimentally measured rotation dynamics and estimated Brownian temperatures of a rotating gold nanorod under varying laser powers. (a) PSD of the backscattered laser light intensity collected by the QPD. (b) Autocorrelation plots of scattering intensity after an analyzer collected by the APD. (c) Laser power-dependent rotation frequencies of nanorods measured by APD and QPD. Error bars reveal the standard deviations of the autocorrelation fitting (red) and of a Lorentzian distribution fit to PSD peak (green), respectively. (d) Power spectrum peak widths of signals shown in (a) and ACF decay rates of signals shown in (b). (e) Estimated T_t and T_r from the experimental corner frequency f_c and ACF decay time τ_0, respectively. Error bars represent 95% confidence intervals. The red solid line indicates the calculated surface temperature of the nanorod while the green solid line indicates the calculated temperature in solution 110 nm away from the nanorod surface. (f) Calculated temperature profile around the gold nanorod when heated by the circularly polarized trapping laser. The yellow and white dashed circles indicate the sizes of the laser beam waist and the movement range of the nanorod center of mass, respectively, with the latter representing two standard deviations of the nanorod displacement.

by $C(\tau) = I_0^2 + 0.5I_1^2 \exp(-\tau/\tau_0) \cos(4\pi f_{avg}\tau)$, where I_0 is the average intensity, I_1 is the amplitude of the intensity fluctuation, and τ_0 is the autocorrelation decay time [19]. The rotational fluctuation is determined by the particle rotational friction coefficient γ_r and the effective rotational Brownian temperature through $\tau_0 = \gamma_r/(4k_B T_r)$, and it relates to the PSD rotational peak width as $\Gamma = (\pi\tau_0)^{-1}$.

We measured the PSD and ACF of a trapped rotating nanorod as a function of applied laser power [Figs. 2(a) and 2(b)]. As indicated previously, the average rotation frequency, f_{avg}, can be obtained either by analyzing the PSD obtained from the QPD data or by analyzing the ACF of the APD signal. Figure 2(c) demonstrates that the two measurements are in excellent agreement. Moreover, the rotation fluctuations estimated from the ACF decay rate and the PSD peak width also match well with each other [Fig. 2(d)]. The agreements is in principle not surprising since both measurements record the scattering intensity of the rotating nanorod after a polarizer, and the PSD of a signal essentially is the Fourier transform of the ACF of the same intensity–time series.

We are now able to analyze the four parameters σ, f_c, f_{avg}, and τ_0 (or Γ):

$$\begin{cases} \sigma = (k_B T_t/k)^{1/2} \\ f_c = k/(2\pi\gamma_t(T_t)) \\ f_{avg} = M_{opt}/(2\pi\gamma_r(T_r)) \\ \tau_0 = \gamma_r(T_r)/(4k_B T_r) \end{cases} \quad (1)$$

which are all directly or indirectly dependent on temperature [19,35,36].

The friction coefficient temperature dependence can be found in Section 2 of Supplement 1. To estimate T_t and T_r, we proceed as follows: We first note that, for given laser properties, the optical driving torque M_{opt} and the trap stiffness k are only determined by the nanorod resonance properties, which are strongly dependent on the rod size and shape. The two friction coefficients, γ_t and γ_r, are also strongly size-dependent. However, the exact size of the trapped nanorod is unknown in the experiments. We first solved the equations of f_{avg} and τ_0 to obtain T_r and the nanorod length from the measured (f_{avg}, τ_0) at a specific laser power $P = 6.4$ mW by assuming that the nanorod diameter is fixed at 84 nm. With the derived particle size, we next calculated T_t and T_r versus laser power from the measured (f_c, τ_0). Figure 2(e) shows that T_t and T_r both increase with laser power. It is also clear that we always have $T_t < T_r$. This is expected for a particle performing hot Brownian motion because the fluid velocity field affecting rotational motion is more localized near the hot particle surface than the velocity field affecting translation [28].

The T_t and T_r values we extract from the preceding experiment are crucial to understanding the non-equilibrium dynamics of a trapped nanoparticle. However, it is not obvious how they relate to the exact temperature distribution around the particle, although we can assume that T_t is basically set by the distribution of temperature within the volume of water that has to move away from the particle as it moves forward through the liquid [27], while T_r is mostly dependent on the properties of the solution very close to the particle surface. To investigate this, we calculated the temperature profile around a trapped nanorod, assuming the same particle and trapping parameters as before, using finite element simulations (FEM, COMSOL Multiphysics) as shown in Fig. 2(f). Figure 2(e) shows that the calculated temperatures
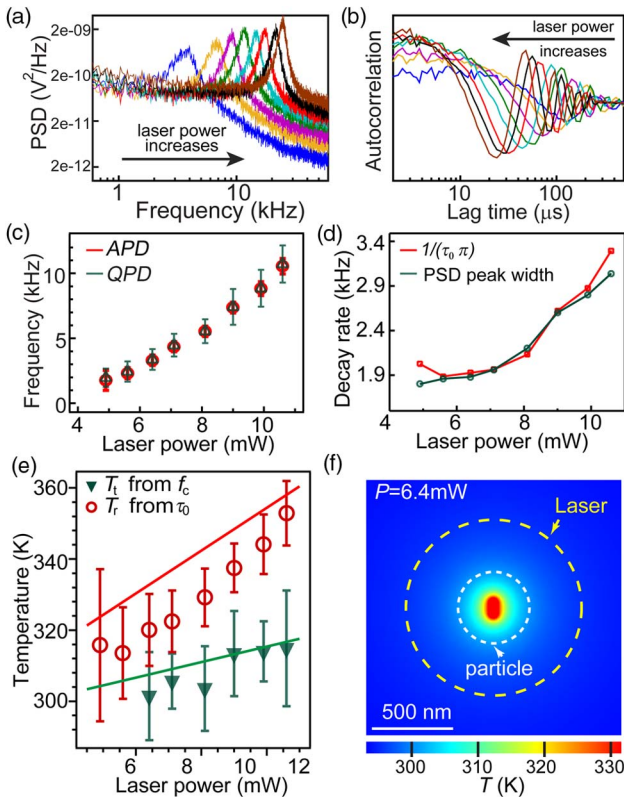
on and 110 nm away from the nanorod surface are very close to the measured T_r and T_t at the same laser power. A slight deviation is not surprising given the uncertainty in particle properties mentioned previously. In any case, the fast temperature drop away from the nanorod surface seen in Fig. 2(f) qualitatively explains why $T_t < T_r$.

3. SIMULATION OF HOT BROWNIAN MOTION

In the analysis of the preceding experimental results, we have implicitly assumed that the translational and rotational Brownian dynamics describes independent degrees of freedom. However, since the nanorod is significantly smaller than the laser spot, its translational motion will lead to a spatially varying optical torque and, hence, a fluctuation in the nanorod rotation frequency *irrespective* of the rotational Brownian motion. The nanorod T_t thus also contributes in the measured T_r. To investigate this effect in more detail, we turn to numerical simulations.

The (angular) velocities of hot Brownian nanoparticles are Maxwell–Boltzmann distributed according to nonuniversal effective temperatures [29]. This allows for an effective equilibrium description in terms of Langevin equations. Since the optical heating affects the translational and rotational movements differently due to the intrinsic nonequilibrium nature of the phenomenon, the translational and rotational effective Brownian temperatures have different values, as also observed in our experiments. For simplicity we still denote the two effective Brownian temperatures by T_t and T_r. We should always have $T_0 \leq T_t \leq T_r \leq T_s$, where T_0 is the ambient temperature and T_s is the nanorod surface temperature [28]. Given that the rod is trapped in 2D and rotating continuously, we assume that its in-plane translational motion is isotropic. The nanorod translational and rotational motions can then be modeled by the following Langevin equations [19,36,37]:

$$m\ddot{x}(t) = -\gamma_t \dot{x}(t) + k_x x(t) + (2k_B T_t \gamma_t)^{1/2} W_x(t),$$

$$m\ddot{y}(t) = -\gamma_t \dot{y}(t) + k_y y(t) + (2k_B T_t \gamma_t)^{1/2} W_y(t),$$

$$J\ddot{\varphi}(t) = -\gamma_r \dot{\varphi}(t) + M_{opt} + (2k_B T_r \gamma_r)^{1/2} W_\varphi(t). \quad (2)$$

Here, x and y are the in-plane particle positions, φ is the rotation angle, m and J are the mass and moment of inertia, γ_t and γ_r are the translational and rotational friction coefficients [38] as before, and $k_x = k_y = k$ are the trap stiffnesses along the two lateral directions. $(2k_B T_t \gamma_t)^{1/2} W_{x,y}(t)$ and $(2k_B T_r \gamma_r)^{1/2} W_\varphi(t)$ are the fluctuating translational force and thermal stochastic torque, respectively, due to random impulses from the fluid molecules [39,40].

Equation (2) can be solved numerically through a Brownian dynamics simulation under the non-inertial approximation (m and J set to zero). The continuous-time solution is then approximated by discrete-time sequences x_i, y_i, φ_i at $t_i = i\Delta t$, where Δt is assumed to be much larger than the friction relaxation times [37]:

$$x_i = x_{i-1} - (kx_{i-1}/\gamma_t)\Delta t + (2D_t \Delta t)^{1/2} w_{i,x},$$

$$y_i = y_{i-1} - (ky_{i-1}/\gamma_t)\Delta t + (2D_t \Delta t)^{1/2} w_{i,y},$$

$$\varphi_i = \varphi_{i-1} - \frac{M_{opt}(x_{i-1}, y_{i-1})}{\gamma_r} \cdot \Delta t + (2D_r \Delta t)^{\frac{1}{2}} w_{i,\varphi}. \quad (3)$$

Here, $w_{i,x}$, $w_{i,y}$, and $w_{i,\varphi}$ are Gaussian random numbers with zero means and unit variances. D_t and D_r are the diffusion coefficients for translational and rotational motions. The discrete

time interval Δt was selected to be much smaller than the time scale on which the restoring force acts, $\phi_t = \gamma_t/k$ [37]. The nanorod was modeled as a prolate ellipsoid for calculating the friction coefficients. All laser trapping parameters, including the laser beam intensity profile, trapping stiffness, and optical torque acting on the nanorod, were selected to mimic actual experimental conditions. Details of the parameter calculations are given in Section 2 of Supplement 1.

A. Translational Fluctuations

We first studied how the temperatures affect the translational motion of the nanorod. According to Eq. (3), only T_t determines the nanoparticle translational motion. We calculated the nanorod trajectory in the optical trap and verified that the rod follows a confined random walk in a potential of $U = kr^2/2$ [Fig. 3(a)]. The particle position exhibits a Gaussian distribution with a standard deviation $\sigma_x = \sigma_y = \sigma = 80.6$ nm [Fig. 3(b)] at $T_t = 293.15$ K. In Fig. 3(c), we also plot the PSD of the particle x-displacement, which can be fitted by $P(f) = C/(f^2 + f_c^2)$ [42] to obtain a corner frequency $f_c = 91.8 \pm 8.2$ Hz. The values of both σ and f_c agree well with those predicted from Eq. (1): $\sigma = 81.6$ nm and $f_c = 93.5$ Hz. We further varied T_t and acquired the corresponding σ_x and f_c by fitting the calculated probability distribution histogram and the PSD of x. Both σ_x and f_c increase with T_t for constant laser power [Figs. 3(d) and 3(e)].

B. Rotational Fluctuations

We next investigate how the temperatures affect the rotational motion of a nanorod. As mentioned previously, the nanorod will feel different optical driving torques when it moves within
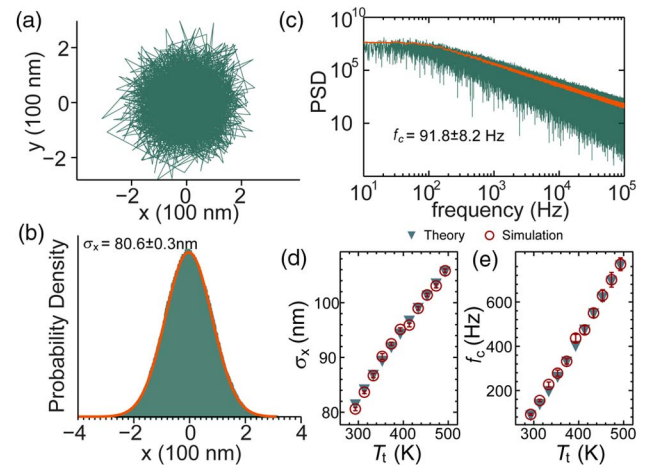

Fig. 3. Simulation of the translational movement of a rotating Brownian gold nanorod in a 2D optical trap. The incident laser power is set to 5 mW. (a) Translational trajectory of the nanorod. (b) Probability distribution of the nanorod position along x. The orange line is a fit to the data using a Gaussian distribution function. (c) Power spectral density (PSD) of the simulated x displacement. The orange line is an averaged PSD obtained using Welch's method to reduce the noise [41]. (d) and (e) x-displacement standard deviation σ_x (d) and PSD corner frequency f_c (e) of the trapped nanorod as the translational effective Brownian temperature T_t varies. The triangles in the plots are calculated from theoretical formulas while the red circles represent the results obtained by fitting the calculated probability distribution and the PSD curve. Error bars in (d) and (e) correspond to 95% confidence intervals obtained from the fits.

the trap, i.e., $M_{\mathrm{opt},i} = M_{\mathrm{opt}}(x_i, y_i)$, because of the Gaussian distribution of the laser intensity. The nanorod thus has continuously varying average rotation frequency $f_{\mathrm{avg},i} = M_{\mathrm{opt}}(x_i, y_i)/(2\pi\gamma_r)$. The probability distribution histogram of f_{avg} [Fig. 4(a)] is consistent with the nanoparticle position probability distribution shown in Fig. 3(b). We computed the rotation frequency and its fluctuation by simulating the experimental measurement, that is, we calculated the intensity of the light scattered from the nanorod after passing through a linear polarizer, $I_{\mathrm{sca},i}^{P} = \sigma_{\mathrm{sca,CP}} I(x_i, y_i) \cos^2 \varphi_i$ [19]. A typical plot of the calculated I_{sca}^{P} is shown in Fig. 4(b), where both T_t and T_r have been set to room temperature by assuming that the particle is not absorbing any energy. The spikes in the curve indicate the fluctuations in the nanorod position and orientation. We then computed the ACF and PSD of I_{sca}^{P}. Curve fitting then gives the nanorod rotation dynamics, f_{avg} and τ_0, as in the experiments.

We next tried to determine the contributions of the nanorod translational and rotational Brownian motion to its overall rotational fluctuation. First, to isolate the translational contribution, the thermal noise term representing the nanorod rotational fluctuation in Eq. (3) is omitted (Section 3 of Supplement 1). The ACF of the calculated I_{sca}^{P} exhibits a well-defined oscillation [Fig. 4(c)] in accordance with the distinct sharp peak that appears in the PSD trace [Fig. 4(d)]. However, the translation dynamics by itself obviously leads to a decaying ACF amplitude and a PSD peak broadening, verifying the fluctuation in the rotation frequency. Note here that the PSD peak exhibits an asymmetry due to the asymmetric rotation frequency distribution [Fig. 4(a)]. Second, in order to instead isolate the contribution from the rotational fluctuation, we assume that the nanorod rotates at a fixed position, namely the laser focus (Section 3 of Supplement 1). This also results in ACF decay and PSD peak broadening, as expected [Figs. 4(c) and 4(d)]. However, note that the peak is now symmetric since the rotational speed fluctuation follows the Maxwell–Boltzmann velocity distribution, and that a corner frequency is not physically defined since the translational motion is excluded from the simulation. Finally, when both translation and rotation are considered, a broader peak can be observed in the PSD and the oscillating amplitude in the ACF decays faster. The extracted rotation frequencies f_{avg} and decay times τ_0 extracted for the three cases (i.e., translations only, rotations only, or both taken into account) are indicated in Fig. 4(c) and found to differ quite significantly. One sees that $f_{t+r} \cong f_t < f_r$, which is expected since $M_{\mathrm{opt}}(0,0) > M_{\mathrm{opt}}$ is always valid. More importantly, we found that $1/\tau_0^{t+r} \approx 1/\tau_0^t + 1/\tau_0^r$. This interesting result holds for a variety of different simulation parameter settings and shows that the translational and rotational contributions to the total ACF decay constant contributes "in parallel". The slight deviation between the left and right sides of the equation comes from the fact that we used the autocorrelation fitting formula to describe the ACFs even though the rotation frequency distribution is not perfectly symmetric. Similarly, the PSD peak widths Γ_t, Γ_r, and Γ_{t+r} are related: $\Gamma_{t+r} \approx \Gamma_t + \Gamma_r$. These results thus indicate that the contributions from translational and rotational Brownian motion to the rotation fluctuations of a trapped particle can, in principle, be clearly separated. Finally, just like in the experiment, we can also obtain T_t and T_r from the simulated particle trajectory data using Eq. (1) and compare these values with the actual input temperatures to Eq. (3). This is further described in Section 4 of Supplement 1. The comparison indicates differences on the order of a few percent or less for the settings used. Specifically, using f_{r+t} and τ_0^{r+t} from the experiment as an approximation to f_r and τ_0^r when calculating T_r leads to a slight underestimation and overestimation, respectively, of the actual effective rotational temperature.

4. CONCLUSION

To summarize, we have shown that by tracking the translational and rotational movements of a spinning gold nanorod optically trapped in 2D, we are able to estimate the translational and rotational effective Brownian temperatures T_t and T_r of the nanorod. The two temperatures differ very significantly due to the optothermal heating of the plasmonic nanoparticle, and they basically agree with average medium temperatures sampled at a distance (~0.1 μm) away from and in very close proximity (~10 nm) to the particle surface, respectively. In the preceding analysis, we have assumed that the dependence of medium viscosity on temperature and the detailed properties of the particle (size, shape, and optical cross-sections) are known. Further, using stochastic simulations, we have shown that translational motion can significantly influence the determination of the rotational Brownian temperature. This effect needs to be considered in all measurements of hot Brownian dynamics of trapped nanoparticles.
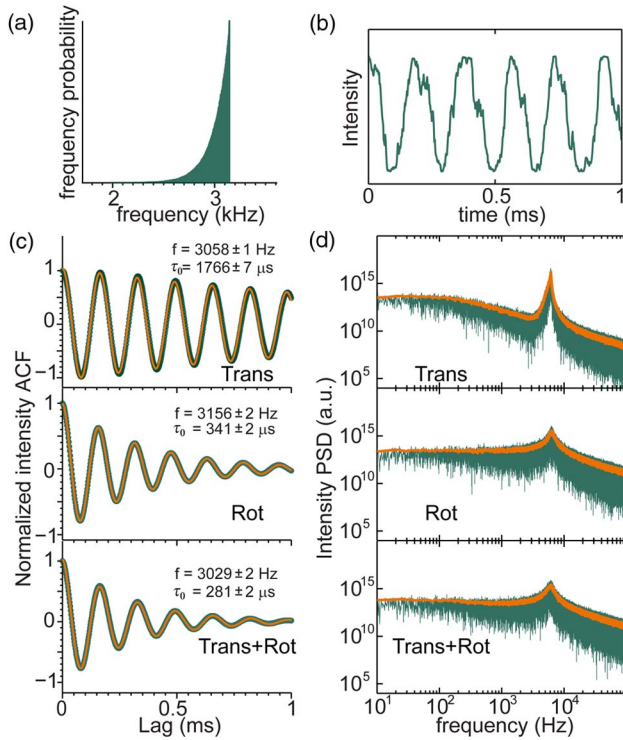

Fig. 4. Simulation results of the rotational movement of a rotating Brownian gold nanorod in 2D optical trap. (a) Probability distribution of the nanorod rotational frequency. (b) Calculated intensity of the scattered light by the nanorod recorded after a polarizer I_{sca}^{P}. The intensity variation indicates the rotational movement of the nanorod. (c) and (d) ACFs (c) and PSDs (d) of the calculated I_{sca}^{P}. The autocorrelation decay and PSD peak broadening result from the rotational fluctuation caused by nanorod Brownian motion. The orange lines in the ACF plots represent fits to the data using the theoretically derived correlation function. The rotation frequency and autocorrelation decay time are obtained from the fitting. The orange lines in the PSD plots are averaged PSDs using Welch's method to reduce the noise [41].

†These authors contributed equally to this work.

See Supplement 1 for supporting content.

REFERENCES

1. M. E. J. Friese, T. A. Nieminen, N. R. Heckenberg, and H. Rubinsztein-Dunlop, "Optical alignment and spinning of laser-trapped microscopic particles," Nature **394**, 348–350 (1998).
2. S. Kheifets, A. Simha, K. Melin, T. C. Li, and M. G. Raizen, "Observation of Brownian motion in liquids at short times: instantaneous velocity and memory loss," Science **343**, 1493–1496 (2014).
3. H. Turlier, D. A. Fedosov, B. Audoly, T. Auth, N. S. Gov, C. Sykes, J.-F. Joanny, G. Gompper, and T. Betz, "Equilibrium physics breakdown reveals the active nature of red blood cell flickering," Nat. Phys. **12**, 513–519 (2016).
4. D. G. Grier, "A revolution in optical manipulation," Nature **424**, 21–22 (2003).
5. G. Volpe and D. Petrov, "Torque detection using Brownian fluctuations," Phys. Rev. Lett. **97**, 210603 (2006).
6. A. I. Bishop, T. A. Nieminen, N. R. Heckenberg, and H. Rubinsztein-Dunlop, "Optical microrheology using rotating laser-trapped particles," Phys. Rev. Lett. **92**, 198104 (2004).
7. J. Millen, T. Deesuwan, P. Barker, and J. Anders, "Nanoscale temperature measurements using non-equilibrium Brownian dynamics of a levitated nanosphere," Nat. Nanotechnol. **9**, 425–429 (2014).
8. K. Neupane, D. A. Foster, D. R. Dee, H. Yu, F. Wang, and M. T. Woodside, "Direct observation of transition paths during the folding of proteins and nucleic acids," Science **352**, 239–242 (2016).
9. K. C. Neuman and A. Nagy, "Single-molecule force spectroscopy: optical tweezers, magnetic tweezers and atomic force microscopy," Nat. Methods **5**, 491–505 (2008).
10. J. R. Moffitt, Y. R. Chemla, S. B. Smith, and C. Bustamante, "Recent advances in optical tweezers," Ann. Rev. Biochem. **77**, 205–228 (2008).
11. K. Svoboda and S. M. Block, "Optical trapping of metallic Rayleigh particles," Opt. Lett. **19**, 930–932 (1994).
12. M. Pelton, M. Z. Liu, H. Y. Kim, G. Smith, P. Guyot-Sionnest, and N. F. Scherer, "Optical trapping and alignment of single gold nanorods by using plasmon resonances," Opt. Lett. **31**, 2075–2077 (2006).
13. L. M. Tong, V. D. Miljković, and M. Käll, "Alignment, rotation, and spinning of single plasmonic nanoparticles and nanowires using polarization dependent optical forces," Nano Lett. **10**, 268–273 (2010).
14. P. V. Ruijgrok, N. R. Verhart, P. Zijlstra, A. L. Tchebotareva, and M. Orrit, "Brownian fluctuations and heating of an optically aligned gold nanorod," Phys. Rev. Lett. **107**, 037401 (2011).
15. A. Ohlinger, A. Deak, A. A. Lutich, and J. Feldmann, "Optically trapped gold nanoparticle enables listening at the microscale," Phys. Rev. Lett. **108**, 018101 (2012).
16. O. M. Maragò, P. H. Jones, P. G. Gucciardi, G. Volpe, and A. C. Ferrari, "Optical trapping and manipulation of nanostructures," Nat. Nanotechnol. **8**, 807–819 (2013).
17. A. Lehmuskero, P. Johansson, H. Rubinsztein-Dunlop, L. M. Tong, and M. Käll, "Laser trapping of colloidal metal nanoparticles," ACS Nano **9**, 3453–3469 (2015).
18. F. Hajizadeh and S. N. S. Reihani, "Optimized optical trapping of gold nanoparticles," Opt. Express **18**, 551–559 (2010).
19. L. Shao, Z.-J. Yang, D. Andrén, P. Johansson, and M. Käll, "Gold nanorod rotary motors driven by resonant light scattering," ACS Nano **9**, 12542–12551 (2015).
20. G. Baffou and R. Quidant, "Thermo-plasmonics: using metallic nanostructures as nano-sources of heat," Laser Photon. Rev. **7**, 171–187 (2013).
21. S. E. Lee and L. P. Lee, "Biomolecular plasmonics for quantitative biology and nanomedicine," Curr. Opin. Biotechnol. **21**, 489–497 (2010).
22. L. Osinkina, S. Carretero-Palacios, J. Stehr, A. A. Lutich, F. Jäckel, and J. Feldmann, "Tuning DNA binding kinetics in an optical trap by plasmonic nanoparticle heating," Nano Lett. **13**, 3140–3144 (2013).
23. J. Croissant and J. I. Zink, "Nanovalve-controlled cargo release activated by plasmonic heating," J. Am. Chem. Soc. **134**, 7628–7631 (2012).
24. L. Shao and J. F. Wang, "Functional metal nanocrystals for biomedical applications," in *Handbook of Photonics for Biomedical Engineering*, A. H.-P. Ho, D. Kim, and M. G. Somekh, eds. (Springer, 2015), pp. 1–32.
25. X. H. Huang, I. H. El-Sayed, W. Qian, and M. A. El-Sayed, "Cancer cell imaging and photothermal therapy in the near-infrared region by using gold nanorods," J. Am. Chem. Soc. **128**, 2115–2120 (2006).
26. M. Braun and F. Cichos, "Optically controlled thermophoretic trapping of single nano-objects," ACS Nano **7**, 11200–11208 (2013).
27. D. Rings, R. Schachoff, M. Selmke, F. Cichos, and K. Kroy, "Hot Brownian motion," Phys. Rev. Lett. **105**, 090604 (2010).
28. D. Rings, D. Chakraborty, and K. Kroy, "Rotational hot Brownian motion," New J. Phys. **14**, 053012 (2012).
29. G. Falasco, M. V. Gnann, D. Rings, and K. Kroy, "Effective temperatures of hot Brownian motion," Phys. Rev. E **90**, 032131 (2014).
30. R. L. Fogel'son and E. R. Likhachev, "Temperature dependence of viscosity," Tech. Phys. **46**, 1056–1059 (2001).
31. C.-K. Chou, W.-L. Chen, P. T. Fwu, S.-J. Lin, H.-S. Lee, and C.-Y. Dong, "Polarization ellipticity compensation in polarization second-harmonic generation microscopy without specimen rotation," J. Biomed. Opt. **13**, 014005 (2008).
32. F. Gittes and C. F. Schmidt, "Interference model for back-focal-plane displacement detection in optical tweezers," Opt. Lett. **23**, 7–9 (1998).
33. F. Hajizadeh, S. M. Mousavi, Z. S. Khaksar, and S. N. S. Reihani, "Extended linear detection range for optical tweezers using image-plane detection scheme," J. Opt. **16**, 105706 (2014).
34. M. Grießhammer and A. Rohrbach, "5D-Tracking of a nanorod in a focused laser beam—a theoretical concept," Opt. Express **22**, 6114–6132 (2014).
35. K. Berg-Sørensen and H. Flyvbjerg, "Power spectrum analysis for optical tweezers," Rev. Sci. Instrum. **75**, 594–612 (2004).
36. A. Lehmuskero, R. Ogier, T. Gschneidtner, P. Johansson, and M. Käll, "Ultrafast spinning of gold nanoparticles in water using circularly polarized light," Nano Lett. **13**, 3129–3134 (2013).
37. G. Volpe and G. Volpe, "Simulation of a Brownian particle in an optical trap," Am. J. Phys. **81**, 224–230 (2013).
38. J. K. G. Dhont, *An Introduction to Dynamics of Colloids* (Elsevier, 1996).
39. S. Chandrasekhar, "Stochastic problems in physics and astronomy," Rev. Mod. Phys. **15**, 1–89 (1943).
40. H. Risken, *Fokker-Planck Equation* (Springer, 1996).
41. P. D. Welch, "The use of fast Fourier transform for the estimation of power spectra: a method based on time averaging over short, modified periodograms," IEEE Trans. Audio Electroacoust. **15**, 70–73 (1967).
42. I. M. Tolić-Nørrelykke, K. Berg-Sørensen, and H. Flyvbjerg, "MatLab program for precision calibration of optical tweezers," Comput. Phys. Commun. **159**, 225–240 (2004).